

# Switching between 3D surface topographies in liquid crystal elastomer coatings using two-step imprint lithography

**Citation for published version (APA):**

Zhang, P., Debije, M. G., de Haan, L. T., & Schenning, A. P. H. J. (2023). Switching between 3D surface topographies in liquid crystal elastomer coatings using two-step imprint lithography. *Small : Nano Micro*, 19(30), Article 2302051. <https://doi.org/10.1002/smll.202302051>

**DOI:**

[10.1002/smll.202302051](https://doi.org/10.1002/smll.202302051)

**Document status and date:**

Published: 26/07/2023

**Document Version:**

Publisher's PDF, also known as Version of Record (includes final page, issue and volume numbers)

**Please check the document version of this publication:**

- A submitted manuscript is the version of the article upon submission and before peer-review. There can be important differences between the submitted version and the official published version of record. People interested in the research are advised to contact the author for the final version of the publication, or visit the DOI to the publisher's website.
- The final author version and the galley proof are versions of the publication after peer review.
- The final published version features the final layout of the paper including the volume, issue and page numbers.

[Link to publication](#)

**General rights**

Copyright and moral rights for the publications made accessible in the public portal are retained by the authors and/or other copyright owners and it is a condition of accessing publications that users recognise and abide by the legal requirements associated with these rights.

- Users may download and print one copy of any publication from the public portal for the purpose of private study or research.
- You may not further distribute the material or use it for any profit-making activity or commercial gain
- You may freely distribute the URL identifying the publication in the public portal.

If the publication is distributed under the terms of Article 25fa of the Dutch Copyright Act, indicated by the "Taverne" license above, please follow below link for the End User Agreement:

[www.tue.nl/taverne](http://www.tue.nl/taverne)

**Take down policy**

If you believe that this document breaches copyright please contact us at:

[openaccess@tue.nl](mailto:openaccess@tue.nl)

providing details and we will investigate your claim.

# Switching between 3D Surface Topographies in Liquid Crystal Elastomer Coatings Using Two-Step Imprint Lithography

Pei Zhang, Michael G. Debije, Laurens T. de Haan,\* and Albert P. H. J. Schenning\*

While dynamic surface topographies are fabricated using liquid crystal (LC) polymers, switching between two distinct 3D topographies remains challenging. In this work, two switchable 3D surface topographies are created in LC elastomer (LCE) coatings using a two-step imprint lithography process. A first imprinting creates a surface microstructure on the LCE coating which is polymerized by a base catalyzed partial thiol-acrylate crosslinking step. The structured coating is then imprinted with a second mold to program the second topography, which is subsequently fully polymerized by light. The resulting LCE coatings display reversible surface switching between the two programmed 3D states. By varying the molds used during the two imprinting steps, diverse dynamic topographies can be achieved. For example, by using grating and rough molds sequentially, switchable surface topographies between a random scatterer and an ordered diffractor are achieved. Additionally, by using negative and positive triangular prism molds consecutively, dynamic surface topographies switching between two 3D structural states are achieved, driven by differential order/disorder transitions in the different areas of the film. It is anticipated that this platform of dynamic 3D topological switching can be used for many applications, including antifouling and biomedical surfaces, switchable friction elements, tunable optics, and beyond.

impacts in tunable optic applications, dynamic antifouling, surface wetting, tribological properties, and directed cell growth, to name a few.<sup>[1–5]</sup> Researchers have been developing synthetic materials, including hydrogels,<sup>[6,7]</sup> shape memory polymers,<sup>[1]</sup> and liquid crystal (LC) polymers<sup>[2,3,8,9]</sup> to achieve switchable surface topographies. For hydrogels, wet environments are typically essential in creating surface structural changes. For shape memory polymers, the surface feature changes are generally one-way: the structured surface will return to the undeformed state when heated but will not revert back to the deformed state when cooled again; additional reprogramming is required to recreate any surface structure.<sup>[1,10–14]</sup>

Using LC polymers, dynamic surface topographies may be generated by programming the LC director distribution, creating material gradients in the plane of the film, or actuating the surface locally.<sup>[2,3,15]</sup> In most cases, the initial rest state of the surface is flat and upon actuation surface structures appear; in other cases the sample presents an initial 3D surface topography,

and upon actuation the topography changes in height.<sup>[2–4,16–21]</sup> LC elastomers (LCEs) with 3D surface pillar array microstructures exhibiting height and diameter changes with changing temperature were created using imprinting or molding

## 1. Introduction


To a great extent, surface topography determines the function of a coating. Dynamic changes of surface topography have significant

P. Zhang, M. G. Debije, A. P. H. J. Schenning  
Stimuli-responsive Functional Materials and Devices (SFD)  
Department of Chemical Engineering and Chemistry  
Eindhoven University of Technology (TU/e)  
Groene Loper, Eindhoven 5600 MB, The Netherlands  
E-mail: a.p.h.j.schenning@tue.nl

M. G. Debije, A. P. H. J. Schenning  
Interactive Polymer Materials (IPM)  
Eindhoven University of Technology (TU/e)  
Groene Loper, Eindhoven 5600 MB, The Netherlands

L. T. de Haan, A. P. H. J. Schenning  
SCNU-TUE Joint Lab of Device Integrated Responsive Materials (DIRM)  
National Center for International Research on Green Optoelectronics  
South China Normal University  
Guangzhou 510006, P. R. China  
E-mail: ldhaan@guohua-oet.com

A. P. H. J. Schenning  
Institute for Complex Molecular Systems (ICMS)  
Eindhoven University of Technology (TU/e)  
Groene Loper, Eindhoven 5600 MB, The Netherlands

 The ORCID identification number(s) for the author(s) of this article can be found under <https://doi.org/10.1002/smll.202302051>

© 2023 The Authors. Small published by Wiley-VCH GmbH. This is an open access article under the terms of the Creative Commons Attribution License, which permits use, distribution and reproduction in any medium, provided the original work is properly cited.

DOI: 10.1002/smll.202302051

methods.<sup>[22–27,28,29]</sup> By programming the LC directors inside the pillars, more complex motions could be achieved.<sup>[30–32]</sup>

Surfaces that transform from one 3D surface topography to a different 3D topography when exposed to stimuli which may reversibly return to their initial state upon removal of the stimuli have not yet been demonstrated. Such dual-structured devices will potentially allow a surface to have different functionalities in the rest and actuated states, broadening the potential applications of dynamic surfaces.

Inspired by the macroscopic shape morphing possible in freestanding films,<sup>[33–37]</sup> we report LCE surface-bound coatings switching between two distinct 3D surface topographies. To make the surface bound films, we use a similar two-step crosslinking process as used in forming the freestanding films.<sup>[33–35,38,39]</sup> First, surface structures are created via imprinting, the resulting surface structured LCEs are partially polymerized into a loose network by an initial crosslinking step. The partially polymerized films then undergo a second imprinting with a second 3D surface structure; the crosslinking of the film is then completed. The resulting LCE coatings show reversible switching between the two embedded, intricate 3D topographies. We foresee this method combining with other approaches, such as patterning of the director distribution or local surface actuation, to enable more interesting, alternating 3D surface structures for application in fields including switchable optics, controllable adhesion, and antifouling.

## 2. Results and Discussion

### 2.1. Fabrication of 3D Surface Topographies

The fabrication of the LCE involves a two-step crosslinking reaction based on an earlier reported LC mixture from White and coworkers (Figure 1A).<sup>[38]</sup> The mixture gives rise to LCE actuation around ambient temperatures. The ratio among the reac-

tive functional groups was kept as thiol: acrylate: vinyl = 1: 0.9: 0.1, so that after the first crosslinking step via the thiol-acrylate Michael addition reaction, there are 10% excess thiol groups remaining. Monomers **1** and **2** are LC diacrylate monomers, which can react with thiol derivatives **3** and **4** through a base catalyzed thiol-acrylate Michael addition. Molecule **6** is used as the base because of its high boiling point. Tetrathiol **4** acts as a crosslinker for this first step, and the ratio between dithiol **3** and tetrathiol **4** was chosen to ensure 10 mol% of thiol groups originating from tetrathiol, forming a loosely crosslinked network after the first crosslinking. In the second crosslinking step via thiol-ene radical photopolymerization, the remaining thiol groups react with the vinyl groups from crosslinker **5**. Molecule **8** is used as an inhibitor to prevent unwanted polymerization between acrylate groups prior to the photopolymerization reaction.

The first surface structure of the LCE is generated via Mold 1 and defines the surface topography in the actuation state (Figure 1B). After the first crosslinking, the surface of the loose network was imprinted using Mold 2 to program a second surface structure and stabilized by fully crosslinking, realizing the surface topography at rest. Heating and cooling of the coating results in switching between the two 3D states (Figure 1C).

### 2.2. LCE Films with Switchable 3D Surface Topographies

First, we verified a surface structure could be imprinted in a free-standing LCE film. A mold (Mold 1) with a grating surface structure with groove periodicity of 6.7 μm and height of 0.35 μm (Figure S1A,B, Supporting Information) was used to create a switchable optical diffraction pattern in the film. The process described in Figure 2A was used to prepare the film: the LC mixture was placed between Mold 1 and a polyvinyl alcohol (PVA) functionalized glass plate with spacers. The cell was maintained at 21 °C overnight to complete the first crosslinking via the base

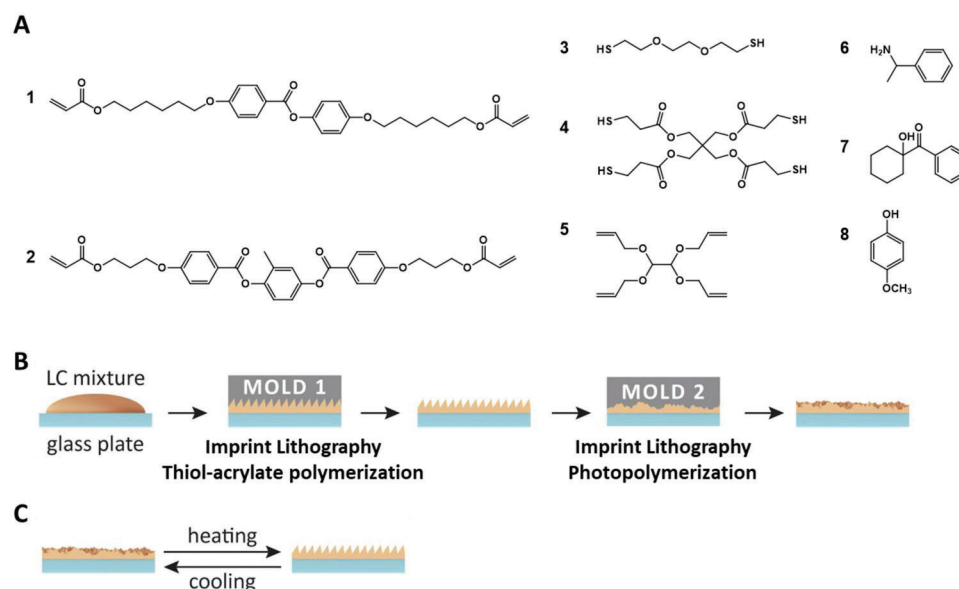


**Figure 1.** A) Chemical structures of the molecules used in this study. B) The process to prepare and program the LCE coating using two-step imprint lithography. C) Schematic illustration of the crosslinked surface topographies switching between two different 3D states upon temperature variation.

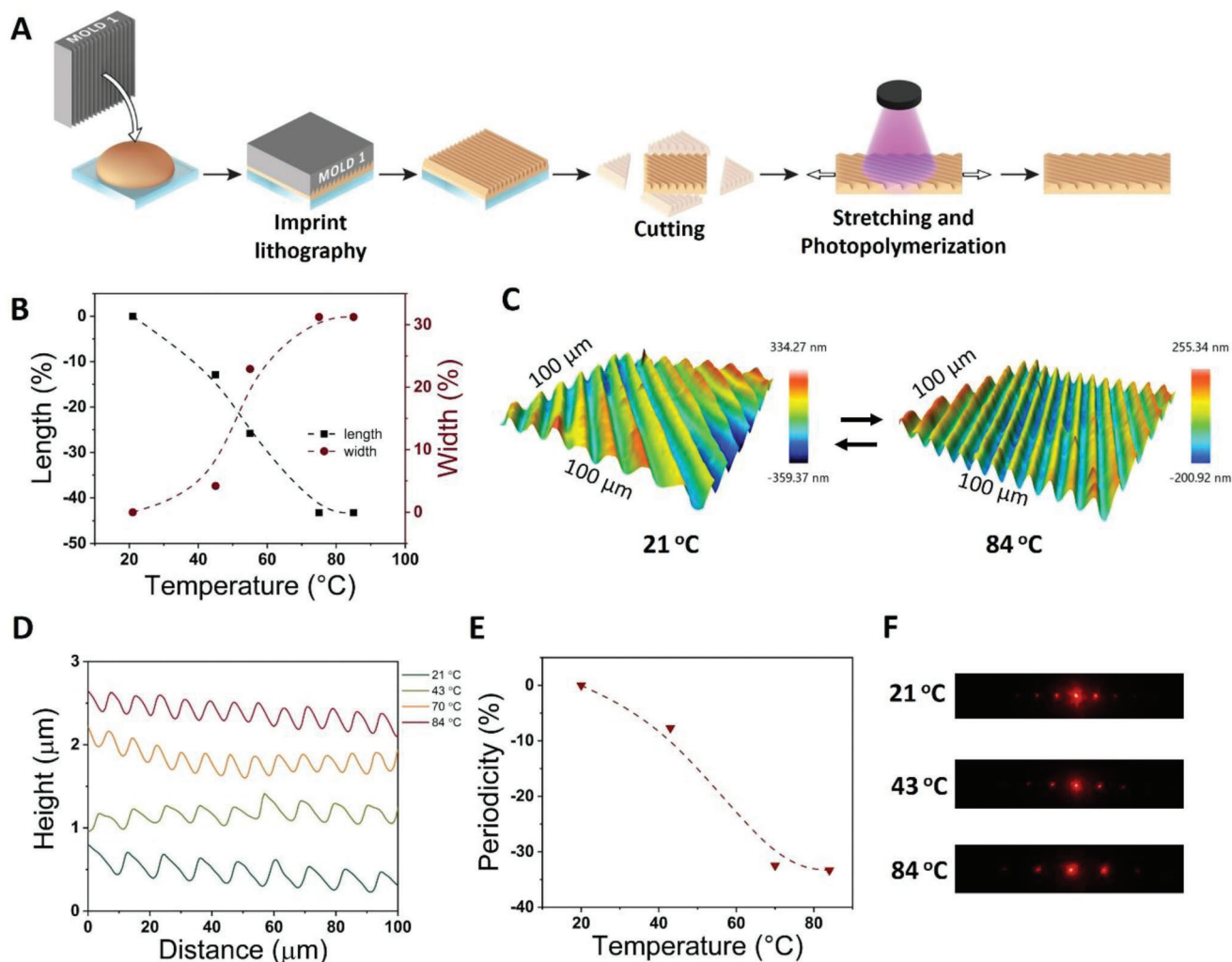


**Figure 2.** LCE film with surface grating structure. A) The process used to prepare freestanding LCE film with surface grating structure. B) Length and width changes of the film as a function of temperature (dashed lines are plotted to guide the eye). C) Topographic images and D) surface profiles of the stretched and photopolymerized LCE film at different temperatures (profiles are y offset from each other for clarity). E) Periodicity of the grating structure as a function of temperature (dashed lines are plotted to guide the eye). F) Diffraction patterns obtained from red laser illumination of the LCE film at different temperatures.

catalyzed thiol-acrylate Michael addition. Mold 1 was removed, and the film was separated from the glass plate by dissolving the PVA in water. Grooves with a periodicity of 6.7  $\mu\text{m}$  and height of 0.22  $\mu\text{m}$  were formed on one side of the film surface (Figure S1C,D, Supporting Information). This surface structure is stabilized by the first crosslinking step, although the height of the grating is lower than in the mold. Differential scanning calorimetry (DSC) reveals a glass transition temperature  $\approx -14.5$   $^{\circ}\text{C}$  and a nematic-to-isotropic transition temperature ( $T_{\text{NI}}$ ) at 40  $^{\circ}\text{C}$  (Figure S2A, Supporting Information).

A uniaxial stretching to a strain of 106% was applied at an angle of  $\approx 45^{\circ}$  to the grating groove direction (Figure S1E, Supporting Information), resulting in the grating periodicity increasing 75% (from 6.7 to 11.7  $\mu\text{m}$ ) and a uniaxial alignment of the mesogens along the stretching direction (Figure S4, Supporting Information). This deformation is fixed by photopolymerization with UV light. The DSC measured after photopolymerization re-

veals a glass transition temperature  $\approx -12$   $^{\circ}\text{C}$  and a  $T_{\text{NI}}$  at 51  $^{\circ}\text{C}$  (Figure S2B, Supporting Information). FTIR of the LCE was measured after both the first and second crosslinking steps (Figure S3A, Supporting Information) and in both FTIR spectra the acrylate peaks disappeared. The stress-strain curves of the LCE films were also measured after both the first and second crosslinking steps and no significant difference was observed between the two curves (Figure S3B, Supporting Information). This suggests that the modulus of the LCE did not undergo a substantial change after fully crosslinking, or too small to be detected with these measurements.

The temperature responsive actuation of the LCE film was characterized. Upon heating and cooling from 21 to 84  $^{\circ}\text{C}$  and back, the film shows a reversible length decrease of 45% and a width increase of 32% as the LCE film passed the  $T_{\text{NI}}$  (51  $^{\circ}\text{C}$ ) (Figure 2B; Figure S1F, Supporting Information), caused by the thermal induced order-to-disorder change (Figure S4,

Supporting Information).<sup>[34,35,38,40,41]</sup> The sample was heated and cooled at least 10 times with no obvious changes in actuation (Figure S1H, Supporting Information). The surface topography of the film was also characterized at different temperatures. The periodicity of the grooves decreases (from 11.7 to 7.8  $\mu\text{m}$ , 33%) upon heating from 21 to 84  $^{\circ}\text{C}$  (Figure 2C,D,E). The change of the surface topography corresponds with the macroscopic changes of the polymer film, revealing that the alternations are related (Figure 2B,E). According to the diffraction equation,<sup>[42,43]</sup> the decrease of periodicity will lead to an increase of diffraction angle. This is demonstrated by shining a laser on this film and measuring the diffraction pattern (Figure 2F; Figure S1G, Supporting Information): the distance between the zeroth and first order diffraction increases upon heating, indicating diffraction angle increases. It is noted that the actuation of this LCE surface topography is also reversible upon cooling (Figure S4, Supporting Information).

### 2.3. LCE Coatings with Switchable 3D Surface Topographies

Having established the responsivity of freestanding films, we looked to reproduce the structural changes for the first time in surface-bound coatings (Figure S5, Supporting Information). To mechanically program the surface topographies in coatings, LCEs chemically bound to a 3-(trimethoxysilyl) propyl methacrylate (silane A174) functionalized glass plate were prepared. The same master grating used to prepare the freestanding LCE film (Figure S1A,B, Supporting Information) was used as Mold 1 (groove periodicity of 6.7  $\mu\text{m}$  and height of 0.35  $\mu\text{m}$ ) to create a LCE coating with a grating surface structure (Figure 3A). After the first crosslinking and removal of the grating mold, grooves with periodicity of 6.7  $\mu\text{m}$  and height of 0.25  $\mu\text{m}$  were measured on the surface of the LCE coating, almost identical to the freestanding LCE film grating (Figure S6A,B vs Figure S1C,D, Supporting Information). Polarized optical microscopy (POM)

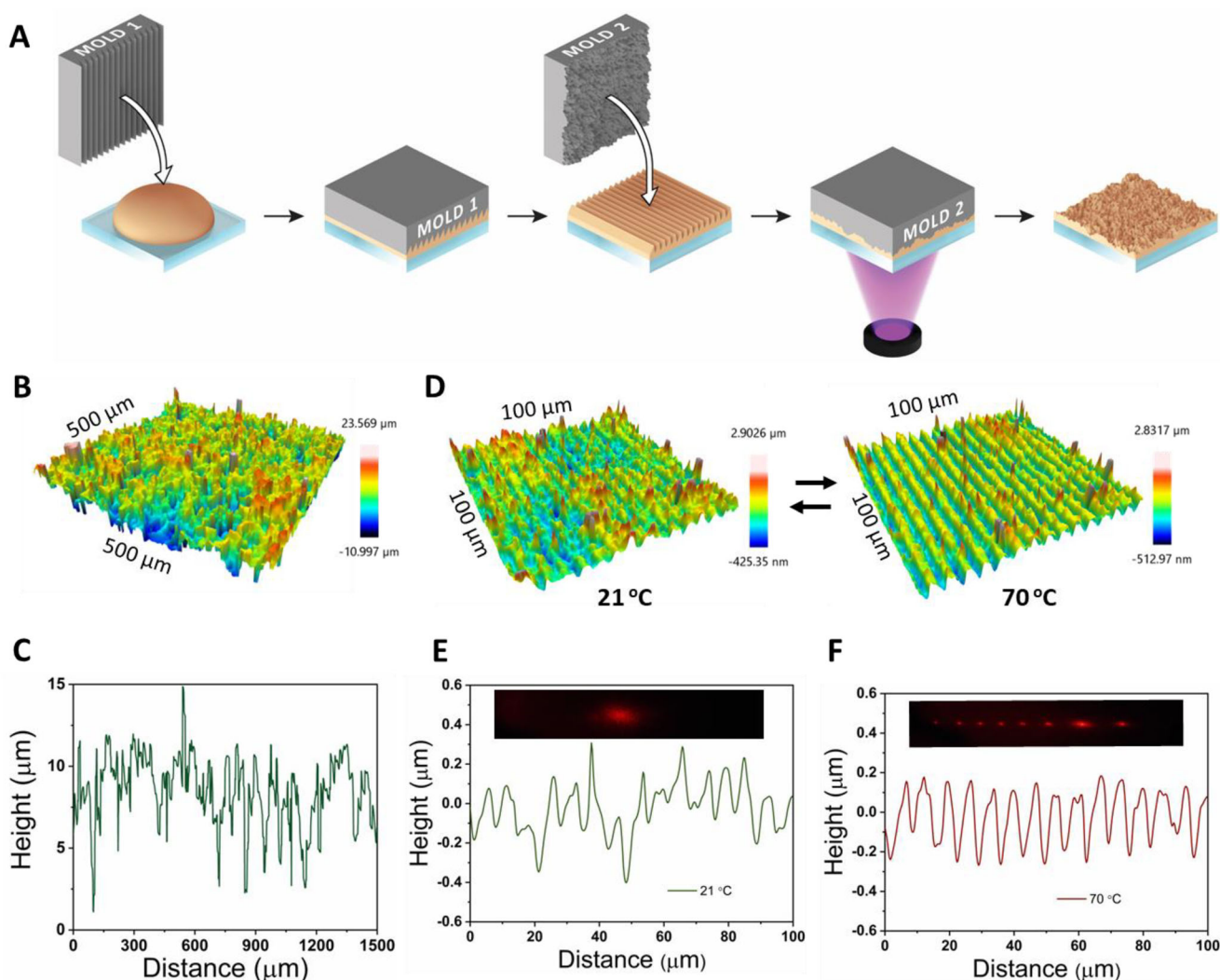


**Figure 3.** LCE coating with surface microstructures switchable between rough and periodic grating structures. A) The process to prepare and program the LCE coating. B) Topographic image and C) surface profile of the rough Mold 2 used to program the surface of the LCE coating during second imprinting. D) Topographic images and E,F) corresponding surface profiles of the coating after being deformed and photopolymerized at different temperatures. The insert photographs in E) and F) are the corresponding diffraction patterns.

image of the coating after first crosslinking reveals the alignment of the coating after first crosslinking being polydomain (Figure S6C, Supporting Information). To program the surface topography for the rest state, a rubberized metal sheet<sup>[44]</sup> with an arithmetic roughness (Ra) of  $\approx 1 \mu\text{m}$  was used as Mold 2 (Figure 3B,C). Mold 2 was intended to disrupt the grating structure, and when brought into contact with the LCE and manually pressed, increased the irregularity of the surface, and the deformation was fixed by photopolymerization. The resulting coating surface is rough and the sample at 21 °C has lost the periodicity of the grating grooves (Figure 3D,E). This near disappearance of the grating structure is verified by POM (Figure S7, Supporting Information). The increase of surface roughness and disappearance of the grating results in disappearance of the diffraction pattern, replaced by light scattering (insert in Figure 3E). Upon heating to 70 °C, the periodic grooves reappeared (Figure 3D,F; Figure S7, Supporting Information) and the coating produces diffraction up to the sixth order. The change of the surface topographies between scattering and diffracting patterns is fully reversible, meaning that when cooled to 22 °C, the surface topography was restored to the rough state and the light diffraction was once again lost (Figure S6D,E, Supporting Information). The surface topological changes are reversible throughout at least five heating and cooling cycles.

To demonstrate the versatility of this two-step imprint lithography method, molds with larger features were used to create dynamic triangular prisms, a structure used for antifouling coatings.<sup>[45,46]</sup> Mold 3 is a negative triangular grooved fluorinated ethylene propylene (FEP) copolymer (triangle widths 38  $\mu\text{m}$ , heights 55  $\mu\text{m}$ , and distance between grooves 58  $\mu\text{m}$ ) (Figure S8A,B, Supporting Information),<sup>[46]</sup> and Mold 4 is a positive triangular prism (Figure S8C,D, Supporting Information). The resulting imprinted LCE structure after first crosslinking was of triangular prisms 37.5  $\mu\text{m}$  wide and 51  $\mu\text{m}$  high, with a distance between prisms (flat “plains”) of 58  $\mu\text{m}$  (Figure S8E,F, Supporting Information). The resulting LCE structured surface is then imprinted by clamping Mold 4 orthogonal to the LCE surface structures (Figure 4A). While mass transport of the partially crosslinked structured film upon application of Mold 4 is limited, at 21 °C the original triangular prism walls of the coating have been locally deformed by Mold 4, resulting in formation of isolated “hills” punctuated by “valleys” in the triangular prism extension direction. The valleys created by Mold 4 displaced material to its surroundings, increasing the height of local plains while anisotropically skewing the peaks of the hills (see Figure 4B). The surface profile perpendicular to the original triangular prisms is defined as profile 1, demonstrating the height difference between the generated hills and intermediate plains. Two surface profiles perpendicular to the imprinted valleys were defined as profiles 2 and 3: profile 2 indicates the height difference between the plains and valleys and profile 3 indicates the height difference between the hills and valleys.

Upon heating from 21 to 84 °C, the surface tends to return to the state generated during the first imprint lithography step. The reversion may be followed in Figure 4B,F: in profile 1, the height difference between the hill and the plains increased from 19.4 to 42  $\mu\text{m}$  (an increase of 22.6  $\mu\text{m}$ , 44% relative to the height

of the triangular prisms) (Figure 4C); in profile 2, the height difference between the valley and the plains decreased from 29.8 to 3.6  $\mu\text{m}$  (a decrease of 26.2  $\mu\text{m}$ , 51% relative to the height of the triangular prisms) (Figure 4D), with the valleys almost disappearing at 84 °C; in profile 3, the height difference between the hill and the valley decreased from 41.1 to 16.1  $\mu\text{m}$  (a decrease of 25  $\mu\text{m}$ , 49% relative to the height of the triangular prisms) (Figure 4E). A video was created from the 3D topographic images at different temperatures to visualize the surface topography changes at different regions (Video S1, Supporting Information). The surface topography fully reverts to the rest state after cooling to 22 °C (Figure S8G, Supporting Information).

To determine if the relative changes in heights of the structures are the result of the changes of either the plains or valleys (or both), we determined the absolute height of the structures relative to the substrate surface in a second heating run (Figure S9, Supporting Information). Examination of the surface height changes showed the height of both the valleys and hills increased, while the height of the plains diminished, contributing to the total surface topography change.

One expects when the triangular prism structure on the LCE coating was deformed by Mold 4, local alignment would be created and fixed by the second crosslinking step. Normally, freestanding samples are stretched to give them alignment before fixing in the second step.<sup>[33–35]</sup> Our stretched freestanding films showed a strain of 45%; for samples confined to the glass substrate, such pre-stretching is not possible. Instead, the application of the mold generates a combination of shear, compression, and local displacement of the material, resulting in localized LCE alignments. We anticipate complex director alignments are generated by the irregular material displacements during imprinting. Directly viewing the surface order generated by the molds is difficult due to the thickness of the underlying bulk LCE, itself mostly unaffected by the mold application. However, normal LCE phase transitions are preserved, as evidenced by the POM images in Figure S10 (Supporting Information). One might then expect a reduced strain in the coating (estimated at 12–30% from Figure S9B,C, Supporting Information) than in well-aligned stretched freestanding films, but the order/disorder transition upon heating the surface structures is more than enough to allow significant actuation. The second crosslinking embeds a type of material “memory”, allowing the material to return to this rest state upon cooling.<sup>[47]</sup>

There are limitations to deforming the LCE coatings; for example, the coating with deformed trapezoidal grooved surface did not fully return to the state generated during the first imprinting lithography, likely because the deformation during the second imprinting lithography was too drastic. It has been reported deformation resulting from strains more than 100% during the second crosslinking step lead to residual strain in the sample above the  $T_{\text{NI}}$ .<sup>[33]</sup> This could explain why the valleys did not fully recover to the undeformed state upon heating. In addition, the mass transfer during second imprinting is currently limited. These strains and mass displacement may be alleviated by adjusting the material characteristics and/or the forces and times used during the imprinting and photopolymerization steps. These factors will be further investigated in future work.

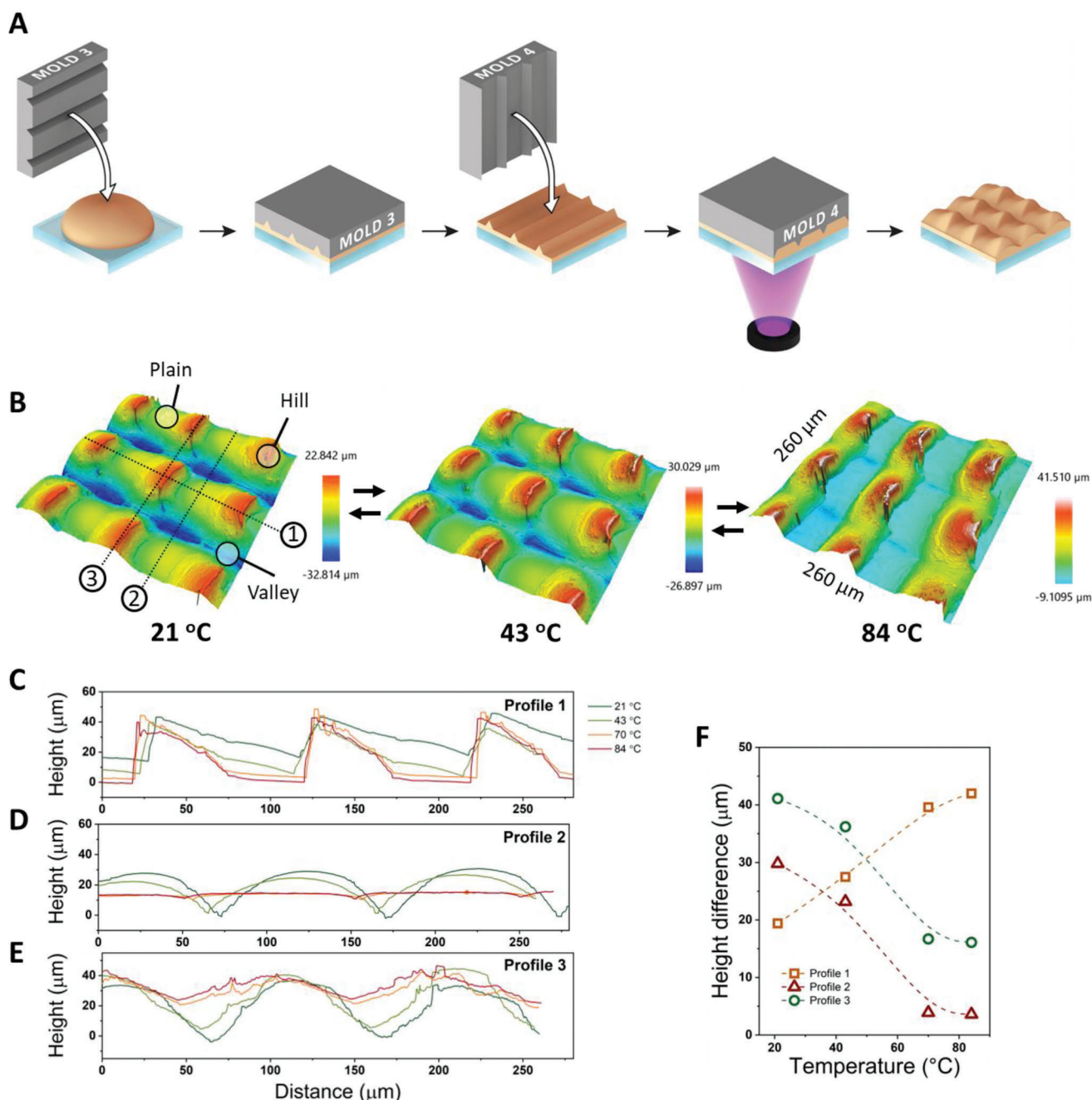


**Figure 4.** LCE coating with surface microstructures switchable between two 3D states. A) The process to prepare and program the LCE coating. B) Topographic images of the coating after being deformed by Mold 4 and photopolymerization at different temperatures. Surface profile 1 (C), 2 (D), and 3 (E) of the LCE coating at different temperatures. F) Surface height differences as a function of temperature (dashed lines are plotted to guide the eye).

### 3. Conclusion

A two-step imprint lithography/crosslinking method was used to create LCE coatings capable of reversibly switching between two distinct 3D surface topographies. First, imprint lithography is used to create 3D microstructure on the coating surface which is partially crosslinked. The resulting surface is imprinted a second time to a second 3D state using a second mold and fixed by a second crosslinking: this second crosslinking appears impor-

tant in enabling totally reversible surface structure changes. By simply changing the molds used in each imprinting step, very different surface structures for both the rest and actuated states were obtained. Surface microstructure switching between rough and periodic gratings were demonstrated, showing the potential of this coating in switchable optics. The second LCE coating used orthogonal imprinting of surface structures to demonstrate switching between quite different surface morphologies. We anticipate the reversible surface microstructure change

between two different 3D states will find use in numerous applications in tunable optics, switchable antifouling, adhesion and wetting surfaces, and in biomedical applications to study cell behaviors in response to topographical changes.

## 4. Experimental Section

**Chemicals and Materials:** Diacrylate LC monomers **1** and **2** were purchased from Daken Chemical. 2,2'-(Ethyleneoxy) diethanethiol (**3**), pentaerythritol tetrakis(3-mercaptopropionate) (**4**), tetrafunctional allyl ether crosslinker (**5**),  $\alpha$ -Methylbenzylamine (**6**), inhibitor 4-Methoxyphenol (**8**), PVA, silane A174 and 1 H, 1 H, 2 H, 2 H – perfluorodecyltriethoxysilane were obtained from Sigma-Aldrich. Photoinitiator (**7**) was obtained from CIBA. FEP copolymer (FEP, TEFLON FEP 100) was purchased from DuPont de Nemours Nederland B.V. All reagents were used as received without further purification.

The grating Mold 1 was obtained from Newport Corporation. The rubberized metal sheet with rough surface was the same as used in a previous study.<sup>[44]</sup> The master brass positive triangular prism mold ( $2 \times 2 \text{ cm}^2$ ) was micro-machined with a triangular diamond cutter. An inverse copy of the microstructures was created from the triangular prism master by mechanically embossing a 10 mm thick FEP sheet with a mechanical embossing apparatus (Tribotrak, DACA) using a load of 5 kg. The system was heated to 270 °C for 30 min and then cooled to room temperature, after which the master was removed and a FEP mold with negative triangular grooved structure was obtained.

**Surface Functionalization:**  $3 \times 3 \text{ cm}^2$  glass plates were cleaned in acetone for 30 min using ultra-sonication and subsequently treated by UV–ozone (PR-100, Ultraviolet Products) for 20 min. To prepare the PVA functionalized glass substrate, 5 wt% PVA with a molecular weight of 9000 was dissolved in distilled water and spin-coated on the clean glass plates using a spin coater (Karl Suss CT 62) by rotating at 2500 rpm for 30 s. The PVA-coated glass plates were then placed on a 60 °C hotplate for 30 min to evaporate the water. To increase the adhesion of the LCE, silane A174 solution (1 vol% in isopropanol/water, v/v = 1:1) was spin coated for 45 s at 3000 rpm on the glass plate. To create a hydrophobic surface for easy removal of the molds after first crosslinking, the master grating was first treated by UV–ozone for 20 min and then dipped in a 1 H, 1 H, 2 H, 2 H – perfluorodecyltriethoxysilane solution (1 vol% solution in isopropanol) for 10 min. Subsequently, the mold was rinsed with isopropanol and placed on a 100 °C hotplate for 10 min.

**Preparation of LCE Films/Coatings:** 13.16 wt% monomer **1**, 57.53 wt% monomer **2**, 22.27 wt% dithiol **3**, 3.32 wt% tetrathiol **4**, 1.73 wt% crosslinker **5**, 1 wt% photoinitiator **7**, 0.5 wt% inhibitor **8** were added to a vial. Around four milliliters of dichloromethane (DCM) were added to the vial to dissolve the solids and ensure good mixing. The vial was magnetically stirred on a 60 °C hotplate around 1.5 h followed by drying in a vacuum oven overnight at 21 °C to remove the DCM. Afterward,  $\approx 300 \text{ mg}$  of the LC mixture was added to a small vial, 2 wt% catalyst **6** was added, and the vial gently heated using a heat-gun and mixed on a vortex mixer to ensure the catalyst was properly blended with the LC mixture. The vial was quickly cooled to room temperature with the help of running water. Around 100 mg of this mixture was placed on a silane A174 functionalized glass plate (or PVA functionalized glass plate for the freestanding films) with pieces of Scotch tape glued onto the edges to serve as spacers (for LCEs with grating structure, spacers of 46  $\mu\text{m}$  were used, and for triangular prisms, spacers of 92  $\mu\text{m}$  were used), and the mold was placed on top to form a cell. Finally, a load  $\approx 690 \text{ g}$  was placed on top of this cell to ensure the structure is properly replicated to the LC. This whole setup was placed at 21 °C overnight to finish the thiol-acrylate Michael addition. Afterward, the mold was removed and a LCE coating with surface structure was obtained. In the case of freestanding LCE films, after removal of the mold, the sample was placed in water at 60 °C for  $\approx 20 \text{ min}$  to remove the PVA functionalized glass plate. The coating/freestanding films were placed at 100 °C for 20 s to remove any deformation created during the mold/substrate removal.

**LCE Surface Programming:** To program the freestanding film surface, the LCE was uniaxially stretched to a specific strain and photopolymerized in a nitrogen box with UV light (300–400 nm) using an Omnicure S2000 UV lamp at an intensity of  $20 \text{ mW cm}^{-2}$  for 10 min on one side; the film was then flipped over and exposed for another 10 min to ensure uniform crosslinking on both sides of the film.

To program the surface of the LCE coating, a second imprinting process was carried out by placing the second mold on top of the LCE coating and pressing either manually or with clamps. The LCE coating was then photopolymerized in a nitrogen box for 20 min to fix the deformation.

**Characterization:** DSC curves were measured with a DSC Q2000 from TA Instruments using rate of  $10 \text{ }^\circ\text{C min}^{-1}$  for both heating and cooling ramps. The surface profile of the LCE coatings/films were measured with a Sensofar 3D optical profilometer using the interferometry technique. Temperature was controlled using a Linkam TMS94 hot stage. To characterize macroscopic actuation, the LCE films were placed on a hotplate, and the length and width of the films were measured. POM images were taken using a Leica DM2700M polarized optical microscope in transmission mode, equipped with a Leica DFC 420C camera. Temperature was controlled using a Linkam THMS600 hot stage. FTIR was measured on a Varian 670-IR FT-IR spectrometer used in transmission mode. The stress–strain curves were performed on LCE films at 21 °C with a TA Instruments Q800 in vertical tension mode at an elongation rate of  $2 \text{ mm min}^{-1}$ . Photographs of the samples were taken with a Sony Cyber-shot camera. To characterize the diffraction pattern of the samples, a 633 nm laser (JDSU Uniphase 1201–2) was used and the diffraction patterns were recorded with a Sony Cyber-shot camera.

## Supporting Information

Supporting Information is available from the Wiley Online Library or from the author.

## Acknowledgements

The authors would like to thank Tom Bus and Sean Lugger for their help with the triangular prism structured molds, Pengrong Lyu for the help with the setup to measure diffraction patterns, Johan Lub for the discussions about the chemicals and ICMS Animation Studio for their help with the 3D illustrations. P.Z. would like to acknowledge the support from the China Scholarship Council.

## Conflict of Interest

The authors declare no conflict of interest.

## Data Availability Statement

The data that support the findings of this study are available from the corresponding author upon reasonable request.

## Keywords

imprint lithography, liquid crystal elastomers, smart coatings, stimuli-responsive polymers, surface topographies

Received: March 22, 2023  
Revised: May 1, 2023  
Published online: May 15, 2023

[1] W. Li, J. Liu, L. Chen, W. Wei, K. Qian, Y. Liu, J. Leng, *Small* **2022**, *18*, 2105958.



- [2] D. Liu, *Adv. Opt. Mater.* **2019**, *7*, 1900255.
- [3] Y. Ji, B. Yang, F. Cai, H. Yu, *Macromol. Chem. Phys.* **2022**, *223*, 2100418.
- [4] *Responsive Polymer Surfaces*, Wiley-VCH, Weinheim, Germany **2017**.
- [5] A. Priimagi, A. Shevchenko, *J. Polym. Sci., Part B: Polym. Phys.* **2014**, *52*, 163.
- [6] C. M. Kolodziej, H. D. Maynard, *J. Am. Chem. Soc.* **2012**, *134*, 12386.
- [7] J. E. Stumpel, D. Liu, D. J. Broer, A. P. H. J. Schenning, *Chem. - A Eur. J.* **2013**, *19*, 10922.
- [8] E. Sungur, M.-H. Li, G. Taupier, A. Boeglin, M. Romeo, S. Méry, P. Keller, K. D. Dorkenoo, *Opt. Express* **2007**, *15*, 6784.
- [9] E. Sungur, L. Mager, A. Boeglin, M.-H. Li, P. Keller, K. D. Dorkenoo, *Appl. Phys. A* **2010**, *98*, 119.
- [10] Z. Cheng, D. Zhang, T. Lv, H. Lai, E. Zhang, H. Kang, Y. Wang, P. Liu, Y. Liu, Y. Du, S. Dou, L. Jiang, *Adv. Funct. Mater.* **2018**, *28*, 1705002.
- [11] A. Belmonte, M. Pilz da Cunha, K. Nickmans, A. P. H. J. Schenning, *Adv. Opt. Mater.* **2020**, *8*, 2000054.
- [12] K. Nickmans, D. A. C. van der Heijden, A. P. H. J. Schenning, K. Nickmans, D. A. C. van der Heijden, A. P. H. J. Schenning, *Adv. Opt. Mater.* **2019**, *7*, 1900592.
- [13] C. A. Tippets, Q. Li, Y. Fu, E. U. Donev, J. Zhou, S. A. Turner, A. M. S. Jackson, V. S. Ashby, S. S. Sheiko, R. Lopez, *ACS Appl. Mater. Interfaces* **2015**, *7*, 14288.
- [14] S. A. Turner, J. Zhou, S. S. Sheiko, V. S. Ashby, *ACS Appl. Mater. Interfaces* **2014**, *6*, 8017.
- [15] K. Mehta, A. R. Peeketi, L. Liu, D. Broer, P. Onck, R. K. Annabattula, *Appl. Phys. Rev.* **2020**, *7*, 041306.
- [16] W. Feng, D. J. Broer, D. Liu, *Adv. Mater.* **2018**, *30*, 1704970.
- [17] T. Takeshima, W. Y. Liao, Y. Nagashima, K. Beppu, M. Hara, S. Nagano, T. Seki, *Macromolecules* **2015**, *48*, 6378.
- [18] G. Babakhanova, T. Turiv, Y. Guo, M. Hendrikx, Q. H. Wei, A. P. H. J. Schenning, D. J. Broer, O. D. Lavrentovich, *Nat. Commun.* **2018**, *9*, 456.
- [19] G. Babakhanova, Y. M. Golestani, H. Baza, S. Afghah, H. Yu, M. Varga, Q. H. Wei, P. Shiller, J. V. Selinger, R. L. B. Selinger, O. D. Lavrentovich, *J. Appl. Phys.* **2020**, *128*, 184702.
- [20] Z. Mahimwalla, K. G. Yager, J. I. Mamiya, A. Shishido, A. Priimagi, C. J. Barrett, *Polym. Bull.* **2012**, *69*, 967.
- [21] J. E. Stumpel, E. R. Gil, A. B. Spoelstra, C. W. M. Bastiaansen, D. J. Broer, A. P. H. J. Schenning, *Adv. Funct. Mater.* **2015**, *25*, 3314.
- [22] Z. Wang, H. Tian, Q. He, S. Cai, *ACS Appl. Mater. Interfaces* **2017**, *9*, 33119.
- [23] J. Lee, Y. Guo, Y. J. Choi, S. Jung, D. Seol, S. Choi, J. H. Kim, Y. Kim, K. U. Jeong, S. K. Ahn, *Soft Matter* **2020**, *16*, 2695.
- [24] J. Cui, D. M. Drotlef, I. Larraza, J. P. Fernández-Blázquez, L. F. Boesel, C. Ohm, M. Mezger, R. Zentel, A. Del Campo, *Adv. Mater.* **2012**, *24*, 4601.
- [25] A. Buguin, M. H. Li, P. Silberzan, B. Ladoux, P. Keller, *J. Am. Chem. Soc.* **2006**, *128*, 1088.
- [26] Y. Hong, A. Buguin, J. M. Taulemesse, K. Kaneko, S. Méry, A. Bergeret, P. Keller, *J. Am. Chem. Soc.* **2009**, *131*, 15000.
- [27] H. Zhao, J. J. Wie, D. Copic, C. R. Oliver, A. Orbaek White, S. Kim, A. J. Hart, *ACS Appl. Mater. Interfaces* **2016**, *8*, 8110.
- [28] Z. L. Wu, A. Buguin, H. Yang, J. Taulemesse, N. Le Moigne, A. Bergeret, X. Wang, P. Keller, *Adv. Funct. Mater.* **2013**, *23*, 3070.
- [29] Z. L. Wu, R. Wei, A. Buguin, J.-M. Taulemesse, N. Le Moigne, A. Bergeret, X. Wang, P. Keller, *ACS Appl. Mater. Interfaces* **2013**, *5*, 7485.
- [30] S. Li, M. M. Lerch, J. T. Waters, B. Deng, R. S. Martens, Y. Yao, D. Y. Kim, K. Bertoldi, A. Grinthal, A. C. Balazs, J. Aizenberg, *Nature* **2022**, *605*, 76.
- [31] R. J. H. van Raak, S. J. A. Houben, A. P. H. J. Schenning, D. J. Broer, *Adv. Mater. Technol.* **2022**, *7*, 2101619.
- [32] Y. Yao, J. T. Waters, A. V. Shneidman, J. Cui, X. Wang, N. K. Mandsberg, S. Li, A. C. Balazs, J. Aizenberg, *Proc. Natl. Acad. Sci. USA* **2018**, *115*, 12950.
- [33] M. Barnes, R. Verduzco, *Soft Matter* **2019**, *15*, 870.
- [34] P. Zhang, G. Zhou, L. T. de Haan, A. P. H. J. Schenning, *Adv. Funct. Mater.* **2021**, *31*, 2007887.
- [35] P. Zhang, M. G. Debije, L. T. De Haan, A. P. H. J. Schenning, *ACS Appl. Mater. Interfaces* **2022**, *14*, 20093.
- [36] M. Yang, Y. Xu, X. Zhang, H. K. Bisoyi, P. Xue, Y. Yang, X. Yang, C. Valenzuela, Y. Chen, L. Wang, W. Feng, Q. Li, *Adv. Funct. Mater.* **2022**, *32*, 2201884.
- [37] Q. He, Z. Wang, Y. Wang, A. Minor, M. T. Tolley, S. Cai, *Sci. Adv.* **2019**, *5*, eaax5746.
- [38] G. E. Bauman, J. M. McCracken, T. J. White, *Angew. Chemie., Int. Ed.* **2022**, *61*, e202202577.
- [39] C. M. Yakacki, M. Saed, D. P. Nair, T. Gong, S. M. Reed, C. N. Bowman, *RSC Adv.* **2015**, *5*, 18997.
- [40] T. J. White, D. J. Broer, *Nat. Mater.* **2015**, *14*, 1087.
- [41] K. M. Herbert, H. E. Fowler, J. M. McCracken, K. R. Schlafmann, J. A. Koch, T. J. White, *Nat. Rev. Mater.* **2022**, *7*, 23.
- [42] C. Palmer, *Diffraction Grating Handbook*, 5th ed., Newport Corporation, New York, USA **2005**.
- [43] R. S. Zola, H. K. Bisoyi, H. Wang, A. M. Urbas, T. J. Bunning, Q. Li, *Adv. Mater.* **2019**, *31*, 1806172.
- [44] K. Nickmans, D. A. C. van der Heijden, A. P. H. J. Schenning, *Adv. Opt. Mater.* **2019**, *7*, 1900592.
- [45] H. O. G. Benschop, A. J. Guerin, A. Brinkmann, M. L. Dale, A. A. Finnie, W. P. Breugem, A. S. Clare, D. Stübing, C. Price, K. J. Reynolds, *Biofouling* **2018**, *34*, 532.
- [46] T. Bus, M. L. Dale, K. J. Reynolds, C. W. M. Bastiaansen, *Biofouling* **2020**, *36*, 138.
- [47] M. Wang, Y. Song, H. K. Bisoyi, J. F. Yang, L. Liu, H. Yang, Q. Li, *Adv. Sci.* **2021**, *8*, 2102674.